Evolution of twist-shear and dip-shear during X-class flare of 13 December 2006: Hinode observations

Sanjay Gosain and P. Venkatakrishnan

Udaipur Solar Observatory,Physical Research Laboratory, Udaipur, Rajasthan- 313 001, INDIA

Received _____; accepted _____

ABSTRACT

The non-potentiality (NP) of the solar magnetic fields is measured traditionally in terms of magnetic shear angle i.e., the angle between observed and potential field azimuth. Here, we introduce another measure of shear that has not been studied earlier in solar active regions, i.e. the one that is associated with the inclination angle of the magnetic field. This form of shear, which we call as the "dip-shear", can be calculated by taking the difference between the observed and potential field inclination. In this *Letter*, we study the evolution of dip-shear as well as the conventional twist-shear in a δ-sunspot using high-resolution vector magnetograms from *Hinode* space mission. We monitor these shears in a penumbral region located close to flare site during 12 and 13 December 2006. It is found that: (i) the penumbral area close to the flaring site shows high value of twist-shear and dip-shear as compared to other parts of penumbra, (ii) after the flare the value of dip-shear drops in this region while the twist-shear in this region tends to increase after the flare, (iii) the dip-shear and twist-shear are correlated such that pixels with large twist-shear also tend to exhibit large dip-shear, and (iv) the correlation between the twist-shear and dip-shear is tighter after the flare. The present study suggests that monitoring twist-shear during the flare alone is not sufficient but we need to monitor it together with dip-shear.

Subject headings: Sun:sunspots-Sun:flares-Sun:magnetic topology

1. Introduction

The deviation of an active region (AR) magnetic field from its potential configuration can arise due to photospheric footpoint motions and/or during flux emergence. However, studies with the high-quality data from space and ground based observatories over the last decade suggest that the latter is more dominant mechanism (Wheatland 2000; Démoulin et al. 2002; Falconer et al. 2002; Leka & Barnes 2003; Schrijver et al. 2005; Jing et al. 2006; Schrijver 2007). The deviation of magnetic field from potential configuration is called non-potentiality (NP) of the field. The magnetic energy of an active region (AR) in excess of the potential magnetic energy is called free magnetic energy (Low 1982). The free magnetic energy of an AR, or a portion of it, is released when flare and/or Coronal Mass Ejections (CMEs) is triggered due to the instability or non-equilibrium (Priest & Forbes 2002). The energy released in the flare is then limited by the amount of free energy or magnetic NP of the AR. Therefore, it is important to characterize the NP of the AR magnetic field in order to predict the intensity of the flare and/or CME.

Traditionally, the so-called magnetic shear i.e., the angle between the observed (ψ_o) and the potential (ψ_p) field azimuths, is used to characterize the NP of the active region magnetic field and is measured as

$$\Delta\psi = \mathrm{acos}\ \frac{\vec{\mathrm{B}}^{\mathrm{o}}_{\mathrm{t}} \cdot \vec{\mathrm{B}}^{\mathrm{p}}_{\mathrm{t}}}{|\mathrm{B}^{\mathrm{o}}_{\mathrm{t}}||\mathrm{B}^{\mathrm{p}}_{\mathrm{t}}|}$$

where $\vec{\mathrm{B}}^{\mathrm{o}}_{\mathrm{t}}$ and $\vec{\mathrm{B}}^{\mathrm{p}}_{\mathrm{t}}$ are the observed and potential transverse field vectors. The term "magnetic shear", used here and in similar studies on solar-magnetism, really refers to "observational shear", which is not to be confused with the actual "shear"–a microscopic property in fluid dynamics. In what follows, we will use the term magnetic shear for traditional reasons and by this term we would always mean the observational shear. Various forms of this parameter are used namely, mean shear (Hagyard et al. 1984), weighted mean shear (Wang 1992), spatially averaged signed shear (Tiwari et al. 2009), most probable

shear (Moon et al. 2003) etc. It is well known that the polarity inversion line (PIL) in active regions bearing highly sheared magnetic fields are the potential sites for flares (Hagyard et al. 1984, 1990). These PILs are generally characterized by dark filaments in the images taken in chromospheric hydrogen alpha line (Zirin & Tanaka 1973).

It may be noted that all of the shear parameters mentioned above measure the twist-shear component of the shear which is measured in the horizontal plane. However, one can also measure the shear of a magnetic field in the vertical plane. This type of shear can be called as the "dip-shear" (we choose the term "dip" because it is synonymous to the dip angle measured in geomagnetism), and can be measured by taking the difference between the observed (γ_o) and the potential field inclination angle (γ_p) i.e., $\Delta\gamma = (\gamma_o - \gamma_p)$.

Physically, the dip-shear can be understood in terms of azimuthal currents, in the same way as the twist-shear is understood in terms of axial currents. In our knowledge, the dip-shear has not been studied earlier in solar active regions. Henceforth, we will call the parameter $\Delta\psi$ and $\Delta\gamma$ and as twist-shear and dip-shear, respectively. The larger the value of these angles the larger will be the NP of the AR. It may be noticed that, unlike twist-shear, the dip-shear is not affected by the 180 degree azimuth ambiguity, provided that the active region is observed close to the disk center. This is because the dip-shear depends upon the inclination angle of the magnetic field which can be measured without ambiguity (Metcalf et al. 2006).

In this *letter*, we study the evolution of twist-shear and dip-shear in a penumbral region located close to the flaring site in AR NOAA 10930. We use sequence of high-quality vector magnetograms observed by the *Hinode* space mission. This active region was in a δ-sunspot configuration which led to a X3.4 flare and a large CME during 02:20 UT on 13 December 2006. The flare was quite powerful and the white light flare ribbons along with impulsive lateral motion of the penumbral filaments were observed (Gosain et al. 2009).

Evolution of the twist-shear and dip-shear together shows interesting patterns which can be distinguished in the pre-flare and post-flare stages. In general we find that (a) the regions with high twist-shear also exhibit high dip-shear, (b) the penumbral region close to the flare site shows high twist-shear and dip-shear, and (c) twist-shear and dip-shear studied together can be used to study flare related changes in the active regions.

The paper is organized as follows. The observational data and the methods of analysis are described in section 2. The results are presented in section 3 and the discussions and conclusions are made in section 4.

2. Observational Data and Methods of Analysis

2.1. Hinode observations

A sunspot with δ configuration was observed in AR NOAA 10930 during 12-13 December 2006 by the Spectro-Polarimeter (SP) instrument (Lites et al. 2007; Ichimoto et al. 2008) with Solar Optical Telescope (SOT) (Tsuneta et al. 2008) onboard *Hinode* satellite (Kosugi et al. 2007). The SP obtains the Stokes profiles, simultaneously in Fe I 6301.5 Å and 6302.5 Å line pair. The spectro-polarimetric maps of the active region are made by scanning the slit across the field-of-view. This takes about an hour to complete one scan. We choose a sequence of six SP scans from 12 December 2006 03:50 UT to 13 December 2006 16:21 UT when the sunspot was located close to the disk center with heliocentric distance (μ) of 0.99 and 0.97, respectively. The scans were taken in "Fast Map" observing mode with following characteristics: (i) Field-of-view (FOV) 295 x 162 arc-sec, (ii) integration time of 1.8 seconds and (iii) pixel-width across and along the slit of 0.32 and 0.29 arc-sec, respectively. The Stokes profiles were then fitted to an analytic solution of Unno-Rachkovsky equations (Unno 1956; Rachkovsky 1973) under the

assumptions of Local Thermodynamic Equilibrium (LTE) and Milne-Eddington model atmosphere (Landolfi & Landi Degl'Innocenti 1982) with a non-linear least square fitting code called *HeliX* (Lagg et al. 2004). The physical parameters of the model atmosphere retrieved after inversion are the magnetic field strength, its inclination and azimuth, the line-of-sight velocity, the Doppler width, the damping constant, the ratio of the line center to the continuum opacity, the slope of the source function and the source function at $\tau = 0$. We fit a single component model atmosphere along with a stray light component. The inversion code *HeliX* is based upon a reliable genetic algorithm (Charbonneau 1995). This algorithm, although slower, is more robust than the classical Levenberg-Marquardt algorithm in the sense that the global minimum of the merit function is reached with higher reliability (Lagg et al. 2004).

The vector magnetograms obtained after inversion, were first solved for 180 degree azimuth ambiguity by using the acute angle method (Harvey 1969) and then transformed from the observed frame (image plane) to local solar frame (heliographic plane) using the procedure described in Venkatakrishnan et al. (1988). The potential field was computed from the line-of-sight field component by using the Fourier transform method (Alissandrakis 1981; Gary 1989). The IDL routine used for potential field computation is `fff.pro` which is available in the NLFFF (Non-linear force free field) package of the SolarSoft library. The continuum intensity images of the sunspot, corresponding to the sequence of scans used, are shown in figure 1, with the transverse field vectors overlaid on it. The two magnetograms were aligned using the cross-correlation technique applied to the continuum image of the sunspot. A black rectangle is overlaid on these images to show the location of the region where we study the evolution of twist-shear and dip-shear. The location of this black rectangle is chosen with the help of a co-aligned G-band filtergram observed from Hinode Filtergraph (FG) instrument during flare. This G-band image is shown in the left panel of figure 2. The flare ribbon is marked by '+' symbols and the black rectangle of figure

1 is shown here also. The flare ribbons sweep across the rectangular box during 02:20 to 02:26 UT. This indicates that the rectangle is chosen such that it samples the penumbra which is very close to the flaring site. The right panel of figure 2 shows the longitudinal magnetogram in order to indicate the location of rectangle (shown here with white color) with respect to the PIL. The maps of dip-shear $\Delta\gamma$ and twist-shear $\Delta\psi$ for the sequence of vector magnetograms are shown in figure 3 and 4 respectively. In figure 5 we show the distribution of dip-shear $\Delta\gamma$ and twist-shear $\Delta\psi$ inside the black rectangle and its evolution with time.

3. Results

3.1. Distribution and Evolution of Non-Potentiality in NOAA 10930

3.1.1. Dip-Shear

The maps of dip-shear $\Delta\gamma$ for the entire sequence of vector magnetograms covering the pre-flare (panels (a)–(c)) and post-flare (panels (d)–(f)) phases are shown in figure 3. The value of field inclination γ is measured with respect to local solar vertical direction and ranges from 0 to 180 degrees. For purely vertical positive (negative) polarity field the value of γ corresponds to 0 degrees (180 degrees). The black rectangle in figure 3 corresponds to negative polarity field. Therefore, the positive value of dip-shear $\Delta\gamma$ inside this rectangle means that the observed field is more vertical than potential field. The magnitude of dip-shear $\Delta\gamma$ can be judged with the aid of colorbar at the bottom of figure 3.

It may be noticed that:

(i) the value of dip-shear $\Delta\gamma$ is large inside the rectangle as compared to other penumbral locations.

(ii) in the pre-flare (panels (a)–(c)) phase the dip-shear $\Delta\gamma$ consistently has a large

magnitude which decreases in the post-flare phase (panels (d)–(f)).

3.1.2. Twist-Shear

The field azimuth has been solved for 180 degree azimuth ambiguity by using the acute angle method (Harvey 1969) and the projection effects have been removed by the application of vector transformation (Venkatakrishnan et al. 1988). This azimuth ambiguity resolution method works well in the regions where the angle $\Delta\psi$ is less or greater than 90°. For regions where $\Delta\psi$ reaches value close to 90° such as along parts of polarity inversion line (PIL) in flaring active regions, the accuracy of the method is poor. This is why we choose a rectangular box for studying the evolution of twist-shear and dip-shear sample the penumbra close to flaring site and at the same time stay away from the PIL where the acute angle method may have problems in resolving the azimuth ambiguity.

The maps of twist-shear $\Delta\psi$ for the entire sequence of vector magnetograms covering the pre-flare (panels (a)–(c)) and post-flare (panels (d)–(f)) phases are shown in figure 4. The value of field azimuth ψ is measured with respect to the positive X-axis and is positive in the anti-clockwise direction. The magnitude of twist-shear $\Delta\psi$ can be judged with the aid of colorbar at the bottom of figure 4. However, for the present study the sign of shear angle is not important, so we shall focus on its magnitude. It may be noticed that the value of twist-shear $\Delta\psi$ is large inside the rectangle and adjacent PIL as compared to other penumbral locations. However, the flare related changes are not so discernable to eye as compared to dip-shear in figure 3.

3.1.3. Evolution of Dip-Shear and Twist-Shear

In figure 5 we show the scatter between the dip-shear $\Delta\gamma$ and twist-shear $\Delta\psi$ for the pixels within the black rectangle shown in previous figures. The panels (a) to (c) correspond to pre-flare while the panels i.e., (d) to (f) correspond to post-flare phase.

It may be noticed that :

(i) The distribution of dip-shear $\Delta\gamma$ and twist-shear $\Delta\psi$ in panels (a)-(c) is different from the distribution in panels (d)-(f).

(ii) The dip-shear increases before the flare (panels (a)-(c)) but twist-shear tends to decrease at the same time.

(iii) The dip-shear and twist-shear are in general correlated, i.e. the pixels with large dip-shear also have large twist-shear.

(iv) The most important change can be noticed after the flare, i.e., between panels (c) and (d). After the flare, (panel (d)) the dip-shear decreases significantly while twist-shear increases. However, now both shear components show less dispersion i.e., follow a tight correlation.

(v) In panels (d)-(f) the two shears maintain smaller dispersion but dip-shear starts to increase once again. This increase suggests that the non-potentiality was building up again in the active region. It may be noted that the flaring activity continued in this region on the next day i.e., 14 December 2006 also, with another X-class flare occurring at about 22:00 UT.

4. Discussion and Conclusion

Hudson (2000) conjectured that the free-energy is stored in non-potential magnetic loops that are stretched upwards and the free-energy release during the flare must be

accompanied by sudden shrinkage or implosion in the field. Also, it is predicted that after the flare the field should become more horizontal (Hudson et al. 2008). Using coronal images during flares, there are observational reports about detection of the loop contraction during flares (Liu et al. 2009).

Further, it was shown by Venkatakrishnan (1990) that in force-free fields a high non-potentiality implies weaker magnetic tension, which in turn implies a larger vertical extension of the field due to lower magnetic pressure gradient. Conversely, the release of free magnetic energy during flare implies a loss of magnetic non-potentiality leading to a decrease in the vertical extension of the field or shrinkage (Forbes & Acton 1996).

The non-linear force-free field (NLFFF) extrapolations of the NOAA 10930 active region by Schrijver et al. (2008) show the non-potentiality of this active region in the form of a twist flux rope structure. As suggested by Venkatakrishnan (1990) and Hudson (2000), such a structure will have larger vertical extension in pre-flare as compared to the post-flare configuration. The closer the post-flare field approaches to the potential field configuration the smaller is the value of inclination difference $\Delta\gamma$ expected. This may give an explanation for the decrease of dip-shear $\Delta\gamma$ after the flare.

However, in contrast, the increase in the twist-shear $\Delta\psi$ after the flare also needs an explanation. The opposite behaviour of twist-shear and dip-shear in relation to the flare can be understood in the following way. The twist-shear is dependent on sub-photospheric / photospheric forces, so the twist-shear will continue to increase independent of coronal processes like flare. However, the plasma β decreases rapidly above the photosphere and thus there is no non-magnetic force or shear that is strong enough to change the inclination of the field lines. Hence inclination will be more responsive to coronal processes. This may explain why inclination became more potential after the flare. Hence, dip-shear could be a better diagnostic of NP above the photosphere.

In summary, we studied the evolution of twist-shear and dip-shear in a flaring δ-sunspot using a sequence of high-quality vector magnetograms spanning the pre-flare and post-flare phases and found that : (i) the penumbra located close to the flaring site has high twist-shear and dip-shear as compared to other parts of the penumbra, (ii) the twist-shear increases after the flare which was earlier reported by Jing et al. (2008) also, (iii) the dip-shear however shows a decrease after the flare, (iv) the twist-shear and dip-shear are correlated, i.e. pixels with high twist-shear exhibit high dip-shear, and this correlation is much tighter after the flare, and (v) distribution of twist-shear and dip-shear and its evolution (in figure 5) clearly shows different patterns before and after the flare.

This type of behaviour in the twist-shear and dip-shear parameters will need to be evaluated further in more flares before it can be understood physically. We plan to carry out more extensive study of the dip-shear and twist-shear in existing *Hinode* datasets. However, a high-cadence study of these shear parameters would be possible only with the upcoming observations from Helioseismic and Magnetic Imager (HMI) onboard Solar Dynamics Observatory (SDO) (Scherrer & SDO/HMI Team 2002). The present study is important in the sense that it points the way to a vector-field follow-up to the results of Sudol & Harvey (2005), which established the line-of-sight field changes during powerful flares.

In the context of present study, one should bear in mind that the vector magnetograms derived from the *Hinode* SOT/SP scans, although polarimetrically very precise are very noisy geometrically. An unwanted consequence of the geometric noise could be that the flows, specially on long time scales, would tend to create an appearance of non-potentiality, even if there was none. This is an important issue which needs to be addressed sooner than later, considering the widespread use of SOT/SP magnetic maps as the "vector magnetograms". We plan to carry out a detailed study of this effect using simultaneously

observed Spectro-Polarimeter (SP) scan from *Hinode* SOT and vector-magnetograms from HMI onboard SDO.

We thank the anonymous referee for his/her valuable comments and suggestions, specially for pointing out the geometric noise in SOT/SP scans and its side effects. We thank Dr. Ron Moore and Dr. Pascal Démoulin for reading the manuscript. Hinode is a Japanese mission developed and launched by ISAS/JAXA, collaborating with NAOJ as a domestic partner, NASA and STFC (UK) as international partners. Scientific operation of the Hinode mission is conducted by the Hinode science team organized at ISAS/JAXA. This team mainly consists of scientists from institutes in the partner countries. Support for the post-launch operation is provided by JAXA and NAOJ (Japan), STFC (U.K.), NASA, ESA, and NSC (Norway). We also would like to thank Dr. Andreas Lagg for providing his HELIX code used in this study.

REFERENCES

Alissandrakis, C. E. 1981, A&A, 100, 197

Charbonneau, P. 1995, ApJS, 101, 309

Démoulin, P., Mandrini, C. H., Van Driel-Gesztelyi, L., Lopez Fuentes, M. C., & Aulanier, G. 2002, Sol. Phys., 207, 87

Falconer, D. A., Moore, R. L., & Gary, G. A. 2002, ApJ, 569, 1016

Forbes, T. G., & Acton, L. W. 1996, ApJ, 459, 330

Gary, G. A. 1989, ApJS, 69, 323

Gosain, S., Venkatakrishnan, P., & Tiwari, S. K. 2009, ApJ, 706, L240

Sudol, J. J., & Harvey, J. W. 2005, ApJ, 635, 647

Hagyard, M. J., Teuber, D., West, E. A., & Smith, J. B. 1984, Sol. Phys., 91, 115

Hagyard, M. J., Venkatakrishnan, P., & Smith, J. B., Jr. 1990, ApJS, 73, 159

Harvey, J. W. 1969, PhD thesis, UNIVERSITY OF COLORADO AT BOULDER.

Hudson, H. S. 2000, ApJ, 531, L75

Hudson, H. S., Fisher, G. H., & Welsch, B. T. 2008, Subsurface and Atmospheric Influences on Solar Activity, 383, 221

Ichimoto, K., et al. 2008, Sol. Phys., 249, 233

Jing, J., Song, H., Abramenko, V., Tan, C., & Wang, H. 2006, ApJ, 644, 1273

Jing, J., Wiegelmann, T., Suematsu, Y., Kubo, M., & Wang, H. 2008, ApJ, 676, L81

Kosugi, T., et al. 2007, Sol. Phys., 243, 3

Lagg, A., Woch, J., Krupp, N., & Solanki, S. K. 2004, A&A, 414, 1109

Landolfi, M., & Landi Degl'Innocenti, E. 1982, Sol. Phys., 78, 355

Leka, K. D., & Barnes, G. 2003, ApJ, 595, 1296

Lites, B. W., et al. 2007, New Solar Physics with Solar-B Mission, 369, 55

Liu, R., Wang, H., & Alexander, D. 2009, ApJ, 696, 121

Low, B. C. 1982, Sol. Phys., 77, 43

Metcalf, T. R., et al. 2006, Sol. Phys., 237, 267

Moon, Y.-J., Wang, H., Spirock, T. J., Goode, P. R., & Park, Y. D. 2003, Sol. Phys., 217, 79

Priest, E. R., & Forbes, T. G. 2002, A&A Rev., 10, 313

Rachkovsky, D. N. 1973, Izvestiya Ordena Trudovogo Krasnogo Znameni Krymskoj Astrofizicheskoj Observatorii, 47, 3

Scherrer, P. H., & SDO/HMI Team. 2002, in Bulletin of the American Astronomical Society, Vol. 34, Bulletin of the American Astronomical Society, 735–+

Schrijver, C. J., De Rosa, M. L., Title, A. M., & Metcalf, T. R. 2005, ApJ, 628, 501

Schrijver, C. J. 2007, ApJ, 655, L117

Schrijver, C. J., et al. 2008, ApJ, 675, 1637

Tiwari, S. K., Venkatakrishnan, P., & Sankarasubramanian, K. 2009, ApJ, 702, L133

Tsuneta, S., et al. 2008, Sol. Phys., 249, 167

Unno, W. 1956, PASJ, 8, 108

Venkatakrishnan, P. 1990, Sol. Phys., 128, 371

Venkatakrishnan, P., Hagyard, M. J., & Hathaway, D. H. 1988, Sol. Phys., 115, 125

Wang, H. 1992, Sol. Phys., 140, 85

Wheatland, M. S. 2000, ApJ, 532, 616

Zirin, H., & Tanaka, K. 1973, Sol. Phys., 32, 173

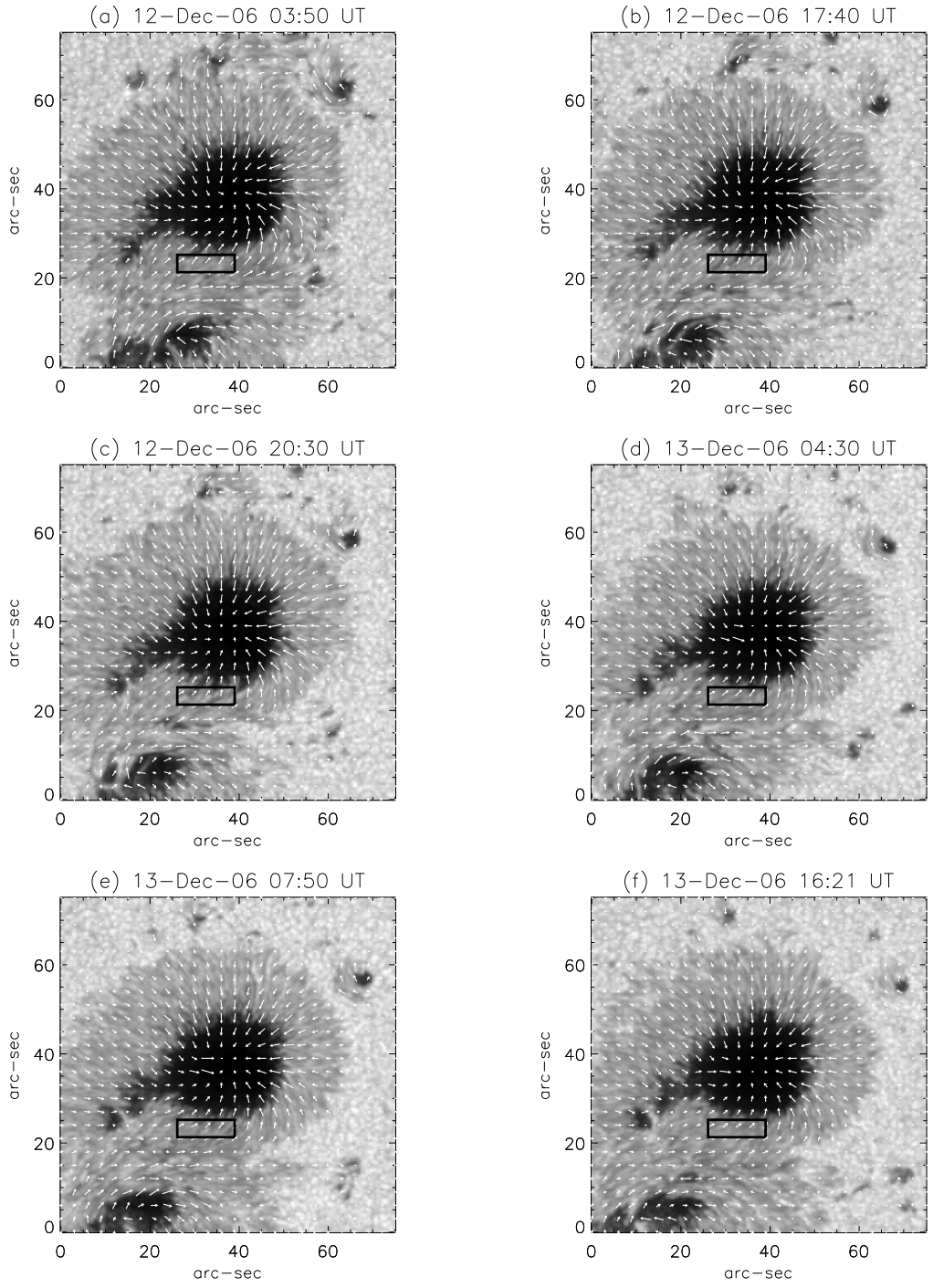

Fig. 1.— The panels (from top to bottom) show continuum intensity map of the δ-sunspot in NOAA 10930 during the times mentioned at the top. The transverse magnetic field vectors are shown by arrows overlaid upon these maps. The black rectangle, shown in all panels, is the region where we monitor the evolution of twist-shear and dip-shear.

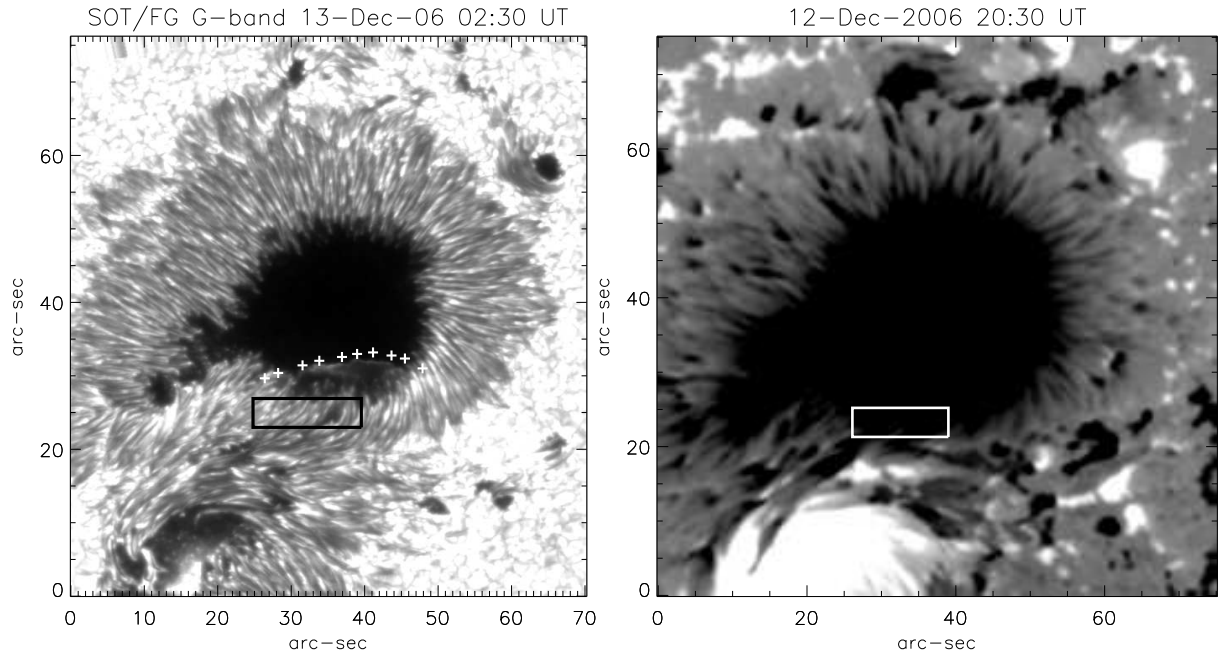

Fig. 2.— The left panel shows the G-band filtergram of the δ-sunspot in NOAA AR 10930 during 12 December 2006 02:30 UT, with the location of the flare ribbon marked by '+' symbols. The flare ribbons sweep across the rectangular box during 02:20 to 02:26 UT. The right panel shows the map of the longitudinal field component for this sunspot. The black (white) rectangle in left (right) panel marks the region where we monitor the evolution of twist-shear and dip-shear.

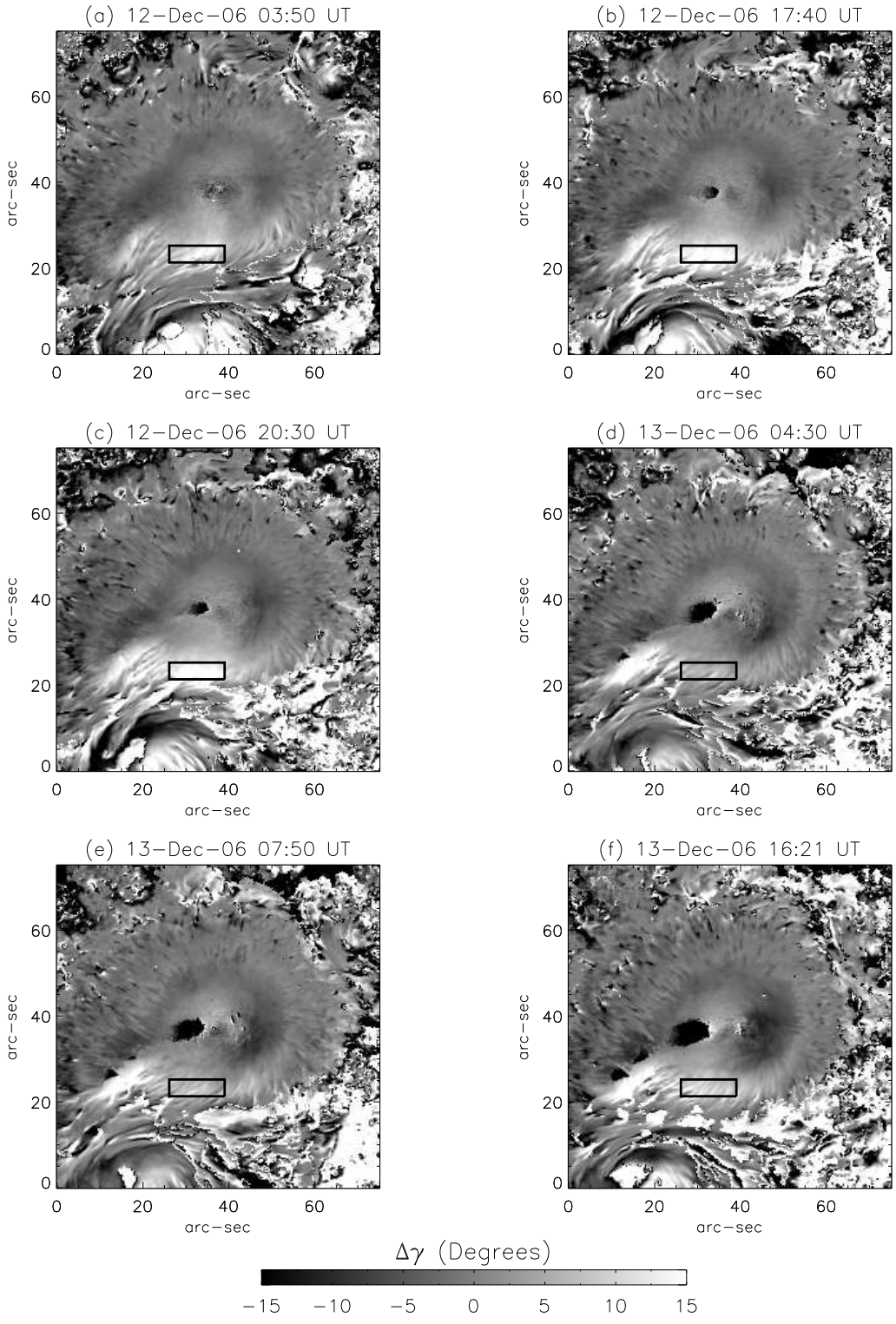

Fig. 3.— The panels (from top to bottom) show the maps of dip-shear, $\Delta\gamma = \gamma_o - \gamma_p$ for NOAA AR 10930 at different times. The black rectangle marks the region where we monitor the evolution of twist-shear and dip-shear.

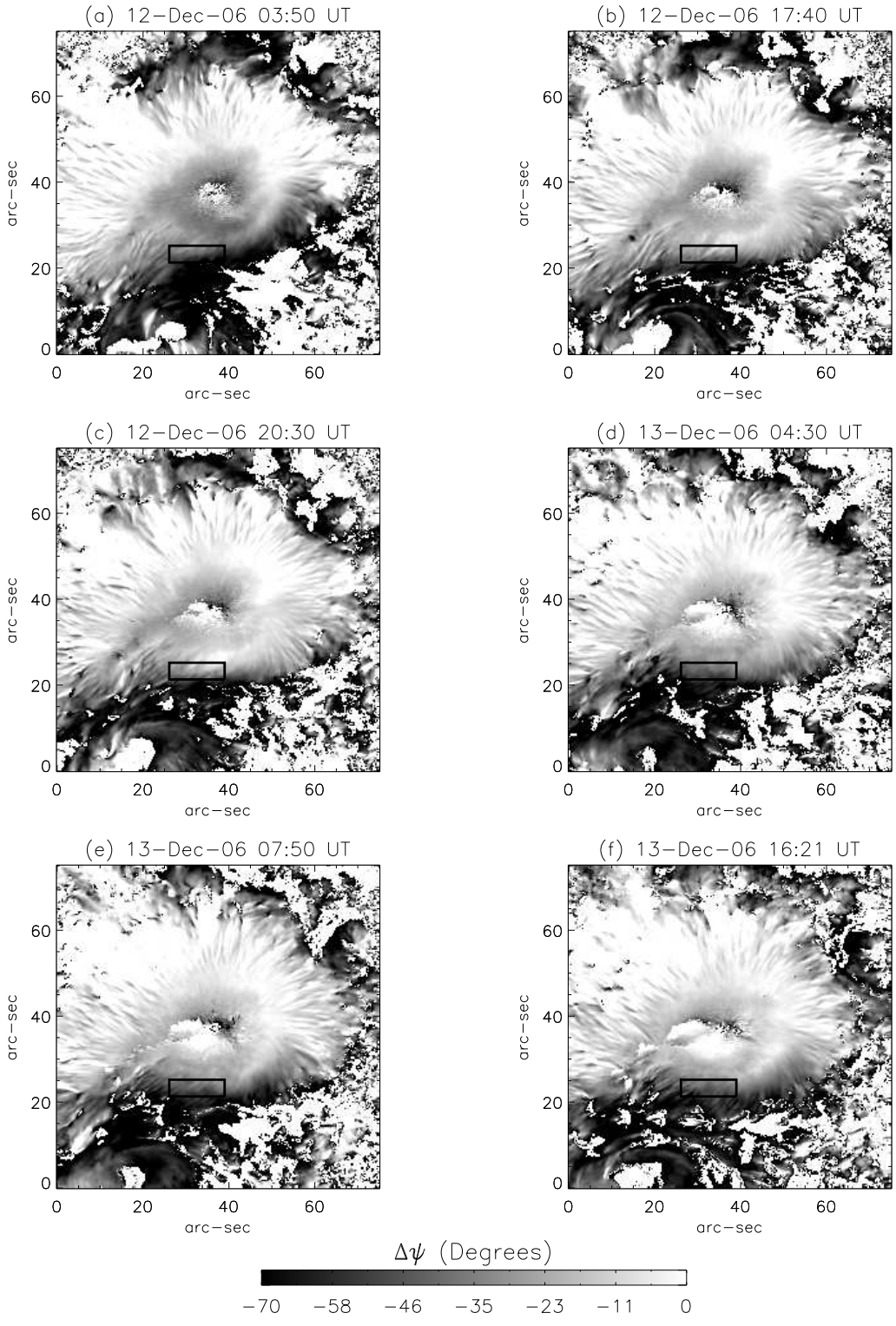

Fig. 4.— The panels (from top to bottom) show the maps of twist-shear, $\Delta\psi = \psi_o - \psi_p$ for NOAA AR 10930 at different times. The black rectangle marks the region where we monitor the evolution of twist-shear and dip-shear.

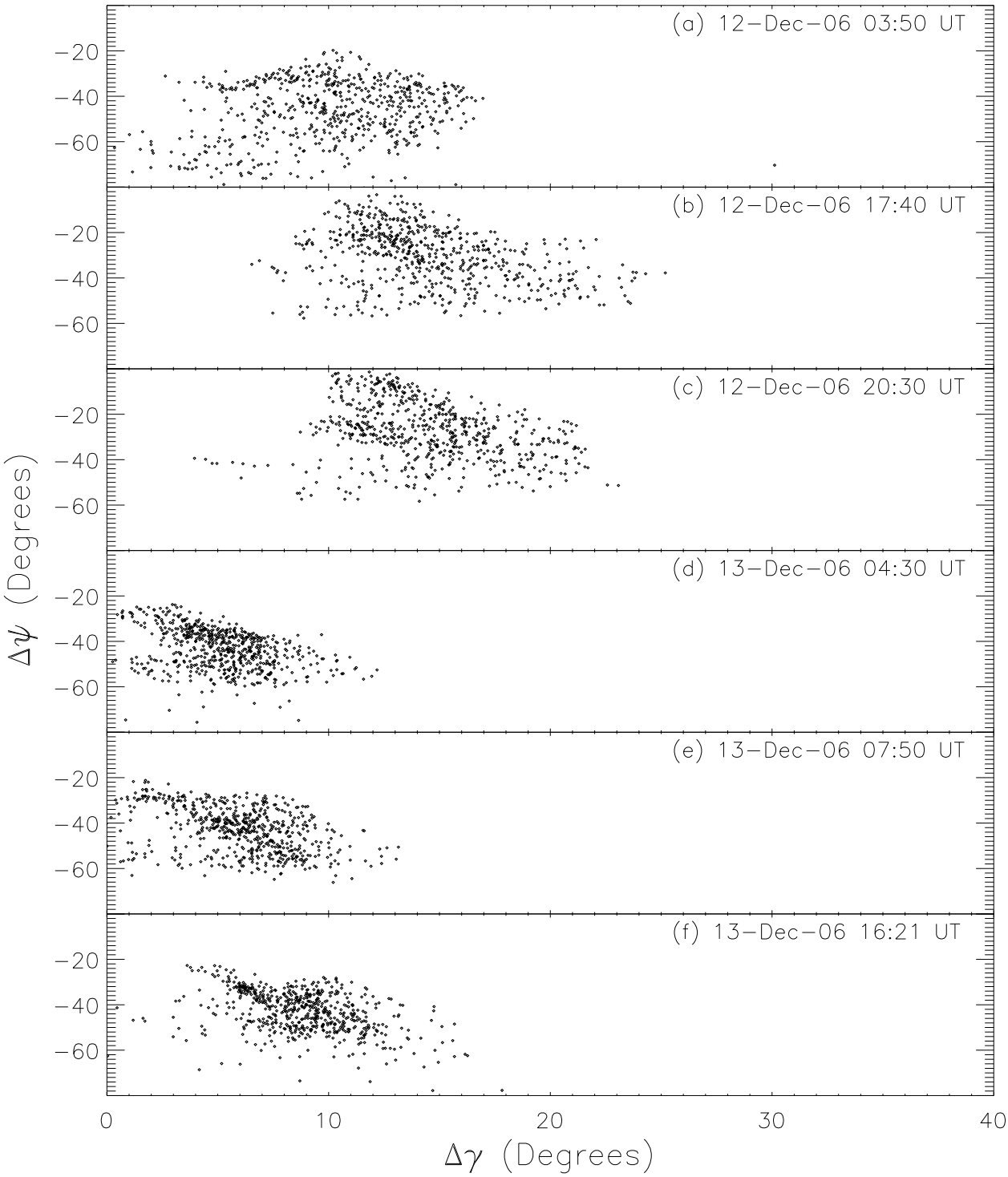

Fig. 5.— The panels (from top to bottom) show the evolution of twist-shear $\Delta\psi$ and dip-shear $\Delta\gamma$ inside the region marked by rectangle in previous figures.